JOURNAL OF SOLID STATE CHEMISTRY 49, 195–205 (1983)

Energy Band Structure and Electronic Transport Properties of Niobium Monoxide[1]

W. E. WAHNSIEDLER

Alcoa Technical Center, Alcoa Center, Pennsylvania 15069

Received April 26, 1983

The energy band structure of niobium monoxide was calculated by Augmented Plane Wave techniques, including detailed calculations of the potential between APW spheres in the lattice. Predictions of isotropic electronic transport parameters were made from the band structure. The results yielded a density of states which was compatible with the X-ray photoelectron spectrum of the material. The band structure was consistent with a material with highly metallic properties. The work function was calculated as 9.4 eV, larger than observed. This difference may be due to an assumed one-electron charge transfer between the Nb and O APW spheres. Hall coefficients calculated from the band structure fell within observed ranges, but transverse magnetoresistances were larger than observed. A variety of possible phenomena were advanced to account for this discrepancy.

Introduction

Niobium monoxide, NbO, exhibits several properties which set it apart from other transition metal oxides and other oxides of niobium. These include high electrical conductivity, a positive temperature coefficient of electrical resistivity (*1*), plasma resonance effects (*2*), large magnetoresistance (*3*), low Peltier coefficient values (*4*), and a silvery luster. These properties (with the exception of large magnetoresistance) are usually associated with metals, not ceramic oxides.

Other calculations of the NbO band structure were carried out by Honig *et al.* (*3*) using the Harrison (*5*) technique, and recently by Wimmer *et al.* (*6*) using the self-consistent Augmented Plane Wave (*7*) technique. Honig and colleagues' largely qualitative results indicated that electrons and holes in several bands were involved in transport phenomena. In this paper a band structure calculation is presented, based primarily on the Augmented Plane Wave technique. This computation has led to a set of dispersion curves along the principal symmetry directions in reciprocal space, and to a density-of-states curve which can be directly compared with spectra obtained from X-ray photoelectron spectroscopy. The dispersion curves serve as a basis for calculating a variety of electronic transport coefficients which can, in some cases, be compared with published experimental results.

Although NbO was first synthesized over 100 years ago (*8*), extensive studies of its physical properties are limited. Work has been reported by Meissner *et al.* (*9*), Pollard (*10*), Pollard and Reed (*11*), Robertson and Rapp (*4*), Honig *et al.* (*1*), and Honig *et al.* (*3*). NbO is stable over a moderately wide stoichiometry range (NbOx, x = 0.98 to 1.03). Many of these studies were based

[1] Supported in part by NSF Grants GH34314 and DMR 79-06886.

0022-4596/83 $3.00

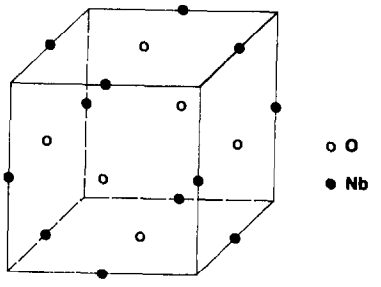

FIG. 1. Crystal structure of NbO.

on nonstoichiometric material. If one excludes nonstoichiometric samples, the remaining data are insufficient to provide a reliable comparison with calculation (which is limited to stoichiometric material by computational constraints). Therefore, comparisons will be made with nonstoichiometric experimental data. Certain of the comparisons seem to suffer from stoichiometric mismatches. These will be noted where they are believed to have occurred.

Calculational Technique

The computational technique described below has been discussed elsewhere in detail (*12*). Readers interested in the computational details of the computer programs used in this work are referred to that source for further information. The overall procedure may be briefly summarized as follows.

The crystal structure of stoichiometric NbO is depicted in Fig. 1. This structure is related to the rocksalt (NaCl) structure by ordered omission of one-third of the anions and cations. The cube edge a in this structure has a length of 4.21 Å. From this known structure, an electronic band structure was derived for noncorrelated electrons using the Augmented Plane Wave (APW) pseudopotential technique (*7*).

The APW matrix elements M^{ij} are given by

$$M^{ij} = \Omega_0(k_j^2 - E)\delta_{ij} - 4\pi \sum_\nu S_\nu^2 \exp(i\mathbf{k}_{ij} \cdot \mathbf{r}_\nu)\, G_\nu^{ij}$$

in which $\mathbf{k}_i$ and $\mathbf{k}_j$ are the wavevectors of two basis functions considered by this matrix element, E is the eigenstate energy, Ω_0 is the volume of the crystal unit cell of the material under consideration, S_ν is the radius of the νth APW sphere, $\mathbf{k}_{ij} = \mathbf{k}_i - \mathbf{k}_j$, $\mathbf{r}_\nu$ is the position vector of the center of the νth APW sphere, and G_ν^{ij} is given by

$$G_\nu^{ij} = (\mathbf{k}_i \cdot \mathbf{k}_j - E) j_1(|\mathbf{k}_{ij}|S_\nu)/|\mathbf{k}_{ij}| - \sum_{l=0}^{l\max} (2l + 1)\, P_l(\hat{k}_i \cdot \hat{k}_j)\, j_l(|\mathbf{k}_i|S_\nu)\, j_l(|\mathbf{k}_j|S_\nu) R_l'(S_\nu)/R_l(S_\nu)$$

in which the P_l's are associated Legendre polynomials, the j_l's are spherical Bessel functions of order l, and R_l' and R_l are, respectively, the derivative (with respect to radius) and the value of the solution to the radial Schrodinger equation inside the νth APW sphere, evaluated at the sphere radius. The sum over ν above is evaluated for each translationally inequivalent APW sphere.

Because of the large volume in the NbO crystal structure which is not occupied by ionic cores (the "vacancies" relative to the NaCl structure), the correction discussed by Loucks (*7*) for varying potential in the "flat potential" APW region outside the spheres was added to the matrix elements above. This correction takes the form

$$\int_{\text{unit cell}} \exp(-i\mathbf{k}_i \cdot \mathbf{r})\, V^\Delta(\mathbf{r}) \exp(i\mathbf{k}_j \cdot \mathbf{r})\, d^3\mathbf{r}$$

in which V^Δ is the deviation of the potential from its average in the "flat potential" region. It was found that this correction was significant.

Charge densities inside the APW spheres were determined according to a self-consistent Dirac equation solution technique of

Liberman *et al.* (*13*). Ionic tailing was treated by Latter's approximation (*14*). A charge transfer of one electronic charge (i.e., Nb^+O^-) was assumed between the anions and cations. This was arrived at by comparison of the electronegativities of Nb and Ti and the self-consistent calculation of Ern and Switendick (*15*) of the APW band structure of TiO. APW lattice potentials were determined according to the technique of Loucks (*7*) for the volume inside the APW spheres. This method evaluates

$$V^{C}_{sph}(\mathbf{r} - \mathbf{r}_\nu) = V^{AT}(\mathbf{r} - \mathbf{r}_\nu) + \sum_{\mu, \text{ all neighbors}} V^{AT}_{sph}(\mathbf{r}_\nu - \mathbf{r}_\mu, \mathbf{r} - \mathbf{r}_\nu)$$

for the νth sphere, in which V^{AT} is the (spherically symmetric) potential for the νth sphere determined according to Liberman *et al.*, and V^{AT}_{sph} is the spherically symmetric component of the potential of the μth sphere, calculated by

$$V^{AT}_{sph}(a,r) = \frac{1}{2ar}\int_{|a-r|}^{a+r} \rho V^{AT}(\rho)d\rho$$

in which $a = |\mathbf{r} - \mathbf{r}_\mu$ and $r = |\mathbf{r} - \mathbf{r}_\nu|$. A similar spherical averaging was carried out to arrive at a spherically symmetric charge distribution inside each APW sphere. This charge distribution was then used to compute the exchange potential, using Slater's free-electron approximation (*16*),

$$V^{X}(\mathbf{r} - \mathbf{r}_\nu) = -6\left(\frac{3}{8\pi}\rho^{C}_{sph}(\mathbf{r} - \mathbf{r}_\nu)\right)^{\frac{1}{3}}$$

and the two potentials were added to form the total potential inside the sphere.

Outside the spheres the potentials from each site were directly summed to arrive at the V^{Δ} function above. The sphere radii were chosen so that the potentials were equal at the sphere tangent points (within the constraints imposed by the radial mesh used in the numerical approximation). In the calculation of lattice potentials, neighbors up to the 14th nearest were treated directly; neighbors further away were treated with the Madelung approximation (*17*).

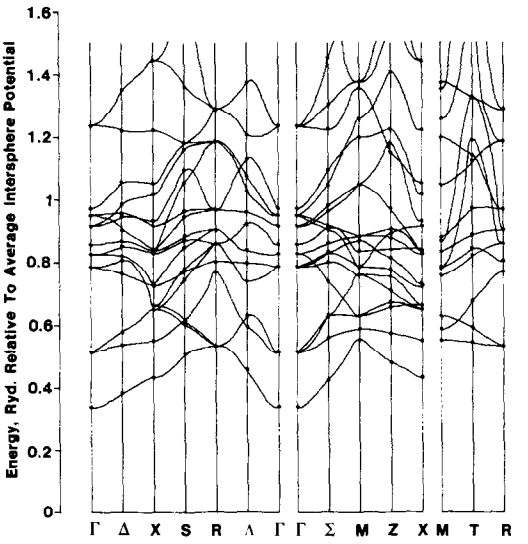

FIG. 2. APW band structure of NbO.

The Loucks procedure, modified by the addition of "vacancy" terms described above, was used to obtain APW eigenvalues along the Δ, Σ, and Λ directions in reciprocal space. The results for all bands above the O-2*p* are depicted in Fig. 2. The connections shown in the figure were arrived at using the compatibility relations (*18*) and the noncrossing rule (*19*).

These eigenvalues were used to construct density-of-states histograms for NbO by dividing the energy range into "panels" and counting the number of eigenstates falling within each panel. Each eigenstate was assumed to carry with it enough eigenstates to fill $\frac{1}{64}$ of the reciprocal unit cell (a total of 64 eigenvalues for each band was generated in the calculations, counting degeneracies). The panel width chosen was the smallest which could be used without introducing large variations in the histogram due to the coarseness of the eigenvalue mesh. The corresponding density-of-states histogram is shown in Fig. 3, smoothed by application

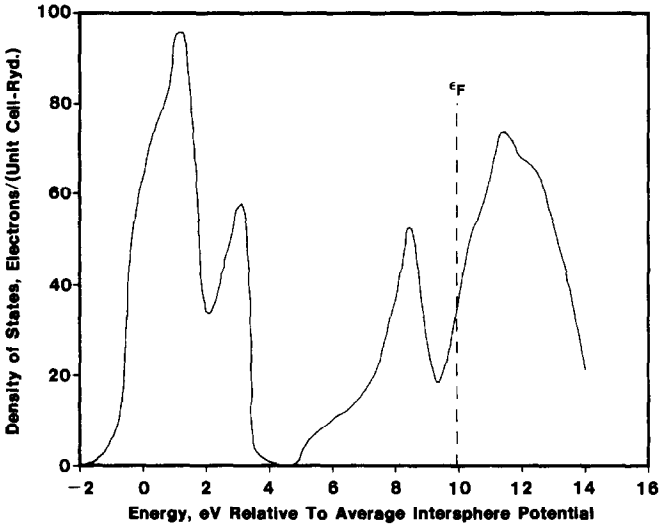

FIG. 3. Calculated density of states of NbO.

of a Gaussian slit function of half-width 2 eV, to simulate instrument resolution. Shifting the panels without changing their width had little effect on the histogram. The Fermi level shown in Fig. 3 (−0.69 Rydbergs relative to free particles) was arrived at by filling eigenstates starting at the bottom of the Nb 4*d* band (above which nine electrons per unit cell must be accommodated).

Electronic transport parameters for NbO were then arrived at using a multiband generalization of the technique presented by Harman and Honig (*20*). This approach evaluates the transport parameters by imposing appropriate experimental constraints on the general transport equation, in matrix form,

$$\begin{pmatrix} J^x \\ J^y \\ J_Q'^x \\ J_Q'^y \end{pmatrix} = \begin{pmatrix} e^2K_1 & Ze^3G_1H_z & \frac{Ze}{T}(K_1\mu_B - K_2) & \frac{e^2H_z}{T}(G_1\mu_B - G_2) \\ -Ze^3G_1H_z & e^2K_1 & -\frac{e^2H_z}{T}(G_1\mu_B - G_2) & \frac{Ze}{T}(K_1\mu_B - K_2) \\ ZeK_2 & e^2G_2H_z & \frac{(K_2\mu_B - K_3)}{T} & \frac{ZeH_z}{T}(G_2\mu_B - G_3) \\ -e^2G_2H_z & ZeK_2 & \frac{-ZeH_z}{T}(G_2\mu_B - G_3) & \frac{(K_2\mu_B - K_3)}{T} \end{pmatrix} \begin{pmatrix} \nabla_x\zeta/e \\ \nabla_y\zeta/e \\ \nabla_x T \\ \nabla_y T \end{pmatrix}$$

in which J^x and J^y are the electron flux in the x and y directions, respectively, $J_Q'^x$ and and $J_Q'^y$ are the heat flux in the x and y directions, and H_z is the magnitude of the magnetic field (assumed to lie along the z axis). T is the temperature, e the electronic charge, Ze the charge of the mobile carriers, and μ_B the carrier band edge energy. ζ

is the Fermi level of the carriers (relative to free particles) and K_i is given by

$$K_i = \frac{-4}{3\hbar^2} \int_{k_{min}}^{k_{max}} \frac{\varepsilon^{i-1}\tau k^2 (d\varepsilon/dk)^2 (\partial f_0/\partial\varepsilon) dk}{(1 + (\omega\tau)^2)}$$

where ε is the carrier energy, τ the relaxation time, f_0 the Fermi–Dirac distribution and ω is given by

$$\omega = \frac{ZeH_z}{\hbar ck} \frac{d\varepsilon}{dk}$$

where c is the speed of light. The G_i are given by

$$G_i = \frac{-4}{3\hbar^2 h^2 c} \int_{k_{min}}^{k_{max}} \frac{\varepsilon^{i-1}\tau^2 k (d\varepsilon/dk)^3 (\partial f_0/\partial\varepsilon) dk}{(1 + (\omega\tau)^2)}$$

where k_{min} and k_{max} are the minimum and maximum wavevectors for which ε is defined for the band being considered.

The method used to arrive at electronic transport parameters utilized an isotropic band structure due to computational limitations. However, spherical averaging of the band structure removed all crossings of the Fermi level. This result is postulated to be due to an unfortunate selection of locations in the reciprocal unit cell for the calculations and to the large number of very localized crossings of the Fermi level which are lost in the averaging process.

To provide a more faithful representation of the electronic behavior, the averaging process carried out on the band structure itself was replaced by averaging of the transport integrals for each direction after the integration process. This procedure permits the integrals to treat more properly the most critical energy regions, namely the areas near the Fermi level. Since the zero-magnetic field electrical conductivity was used as a parameter in the calculation to determine the relaxation time, some correction of inaccuracies in the averaging procedure is afforded by constraining the electrical conductivity to match experiment.

The procedure of Ref. (*20*) was carried out on all bands in which any eigenvalue was within 10 kT (for T = 300 K) of the Fermi level. Six of these bands cross the Fermi level, three do not. Numerical integration of the transport integrals was carried out by fourth-order Gaussian quadrature with the integration panel width equal to 0.16 kT. The results were found to be insensitive to decreasing the panel width and to increasing the order of the quadrature. The band edges were taken as the eigenvalues at the Γ point (zero wavevector) unless an extremum was present in the $\varepsilon(k)$ curve, in which case the extremum was used.

As mentioned above, the experimental zero-field electrical conductivity was used to determine the relaxation time constant τ_0 in the expression

$$\tau = \tau_0 \varepsilon^{r-\frac{1}{2}}$$

in which τ is the relaxation time, ε the electron energy, and r takes integral values between 0 and 2 depending on the scattering mechanism investigated. Results for the three mechanisms are quoted below, based on conductivity values of Pollard and Reed (*11*). Electrons in lower shells were accounted for by an appropriate addition to the wavevector (extended zone scheme). The lattice thermal conductivity was arbitrarily assigned a value of 0.1 of the electronic thermal conductivity at 300 K. No experimental value for the lattice thermal conductivity is available in the literature.

Transport parameters determined by this procedure are given in Table I. In these tables, τ is the relaxation time, σ the transverse electrical conductivity, P the transverse Seebeck coefficient, κ the transverse thermal conductivity, R the isothermal Hall coefficient, η the transverse Nernst coefficient, m the Righi-Leduc coefficient, and J the Ettingshausen coefficient. L is the

TABLE IA

NbO TRANSPORT PARAMETERS AT 100 K[a]

Magnetic field (G)	Parameter	Gaussian units		
		$r = 0$	$r = 1$	$r = 2$
0	τ_0	6.327303E 18	8.355675E 1	1.102327E−15
	σ_0	5.300000E 17	5.300000E 17	5.300000E 17
	P_0	7.170307E −9	7.352868E −9	7.538359E −9
	κ_0	1.476487E 7	1.523745E 7	1.567037E 7
	L	2.786E−13	2.875E−13	2.957E−13
1,000	σ	5.300000E 17	5.300000E 17	5.300000E 17
	P	7.170307E −9	7.352868E −9	7.538359E −9
	κ	1.476487E 7	1.523745E 7	1.567037E 7
	R	5.273750E−26	5.650115E−26	6.026424E−26
	η	−6.782951E−16	−7.203023E−16	−7.620243E−16
	m	1.159289E −7	1.144682E −7	1.132251E −7
	J	−1.406196E−17	−1.337659E−17	−1.275363E−17
100,000	σ	5.299921E 17	5.299921E 17	5.299921E 17
	P	7.169715E −9	7.352245E −9	7.537705E −9
	κ	1.476382E 7	1.523636E 7	1.566923E 7
	R	5.273734E−26	5.650097E−26	6.026404E−26
	η	−6.782603E−16	−7.202646E−16	−7.619837E−16
	m	1.159328E −7	1.144719E −7	1.132287E −7
	J	−1.406291E−17	−1.337751E−17	−1.275452E−17

[a] Exponential notation is used, in which E indicates that the following number is an exponent of 10 which multiplies the preceeding mantissa.

TABLE IB

NbO TRANSPORT PARAMETERS AT 200 K

Magnetic field (G)	Parameter	$r = 0$	$r = 1$	$r = 2$
0	τ_0	2.622245E 18	3.462305E 1	4.566876E−16
	σ_0	2.200000E 17	2.200000E 17	2.200000E 17
	P_0	1.313088E −8	1.337384E −8	1.361209E −8
	κ_0	1.131651E 7	1.167032E 7	1.199262E 7
	L	2.572E−13	2.652E−13	2.726E−13
1,000	σ	2.200000E 17	2.200000E 17	2.200000E 17
	P	1.313088E −8	1.337384E −8	1.361209E −8
	κ	1.131651E 7	1.167032E 7	1.199262E 7
	R	5.305791E−26	5.679447E−26	6.052751E−26
	η	−5.727683E−16	−6.096489E−16	−6.465539E−16
	m	5.383914E −8	5.328983E −8	5.284375E −8
	J	−7.576539E−18	−7.209516E−18	−6.876129E−18
100,000	σ	2.199994E 17	2.199994E 17	2.199994E 17
	P	1.313067E −8	1.337362E −8	1.361186E −8
	κ	1.131636E 7	1.167016E 7	1.199246E 7
	R	5.305788E−26	5.679443E−26	6.052747E−26
	η	−5.727632E−16	−6.096434E−16	−6.465480E−16
	m	5.383951E −8	5.329019E −8	5.284410E −8
	J	−7.576637E−18	−7.209609E−18	−6.876219E−18

TABLE IC
NbO TRANSPORT PARAMETERS AT 300 K

Magnetic field (G)	Parameter	$r = 0$	$r = 1$	$r = 2$
0	τ_0	5.348133E 17	7.059123E 0	9.307873E−17
	σ_0	4.500000E 16	4.500000E 16	4.500000E 16
	P_0	1.752312E −8	1.762629E −8	1.769663E −8
	κ_0	3.498786E 6	3.612786E 6	3.719729E 6
	L	2.592E−13	2.676E−13	2.755E−13
1,000	σ	4.500000E 16	4.500000E 16	4.500000E 16
	P	1.752312E −8	1.762629E −8	1.769663E −8
	κ	3.498786E 6	3.612786E 6	3.719729E 6
	R	5.354544E−26	5.722936E−26	6.090314E−26
	η	−1.785275E−16	−1.905803E−16	−2.027487E−16
	m	1.135412E −8	1.124959E −8	1.116062E −8
	J	−4.969063E−18	−4.719809E−18	−4.489523E−18
100,000	σ	4.500000E 16	4.500000E 16	4.500000E 16
	P	1.752311E −8	1.762627E −8	1.769661E −8
	κ	3.498784E 6	3.612784E 6	3.719726E 6
	R	5.354543E−26	5.722936E−26	6.090314E−26
	η	−1.785274E−16	−1.905803E−16	−2.027487E−16
	m	1.135412E −8	1.124959E −8	1.116062E −8
	J	−4.969965E−18	−4.719812E−18	−4.489526E−18

Lorentz number, defined as

$$L = \frac{\kappa}{\sigma T}$$

which, for a free electron gas, has a value of 2.72×10^{-13} in Gaussian units. Experimental data against which these results can be compared are very limited, but a comparison with what is available is the subject of the following section.

Discussion

It is clear that the large electrical conductivity of NbO is explained by the numerous Fermi level crossings observed in the APW band structure. Both hole and electron type conduction are present in the form of nearly full bands (Λ_1, Σ_2) and nearly empty bands (Λ_3, Δ_5, Δ_2', Δ_1) and one half-full band (Σ_4). Most of the bands crossing the Fermi level do so monotonically, but one band (Λ_3) exhibits an energy minimum just above the Fermi level. This will generate an "electron pocket" at finite temperature. All the partially filled bands can be decomposed into states of predominantly Nb 4*d* character; therefore, most of the electronic conduction in NbO involves 4*d* electrons.

The results of Wimmer *et al.* for the NbO band structure show several similarities to these calculations. The most striking difference between their band structure and the current one is the mixing of the O-2*p* band with the conduction band in their case. The present calculations predict a very small gap between the top of the O-2*p* band and the conduction band. This difference may be due to the lack of self-consistency in the present APW calculation or to the inclusion of a detailed intersphere potential, whereas Wimmer *et al.* used APW spheres to model the potential around the Nb and O "vacancies," thus forcing these potentials to be

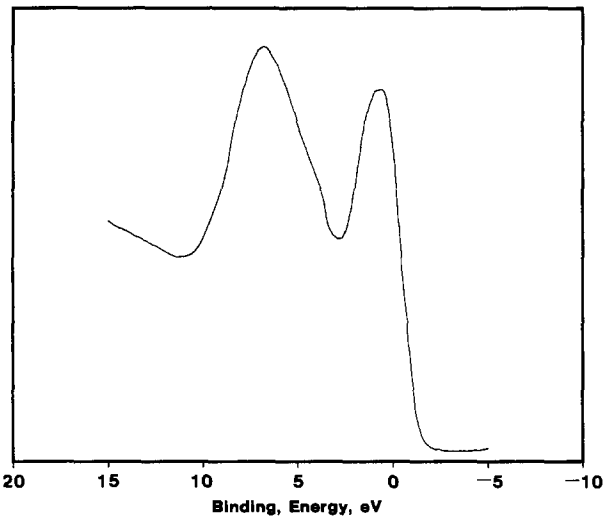

FIG. 4. X-Ray photoelectron spectrum of NbO.

spherically symmetric. Another difference between the two calculations is the use of the Slater free-electron exchange potential in the present work, and the use of the Hedin and Lundqvist potential by Wimmer *et al.*

The results in Table I present a generally metallic picture of the transport parameters of the material. A quantitative calculation of the electrical conductivity was not undertaken due to uncertainties in the degree of the carrier-lattice coupling. Calculation of Hall mobility and carrier density is not warranted because the Hall coefficient is an algebraic sum of the individual contributions of each carrier, and these are of differing sign. This explains the observation that the calculated Hall coefficients are less than those observed in copper. Similarly, the complex band structure makes a simple interpretation of the Seebeck coefficient impossible. For a free electron gas, no change in electrical conductivity should be seen during application of a transverse magnetic field. Indeed, the magnetoresistances calculated are quite small. More will be said about this last point below. The Lorentz numbers calculated agree quite well with that for a free electron gas. The discrepancies are probably due to the complexities of the band structure and the use of a nonconstant relaxation time.

From a computational standpoint, the most basic result against which the results quoted above can be compared is the X-ray photoelectron spectroscopy (XPS) spectrum obtained by Honig *et al.* (*21*). This spectrum is approximately proportional to the electronic density-of-states below the Fermi level. The XPS spectrum results are shown in Fig. 4. There is a striking similarity in the appearance of Figs. 3 and 4. Comparison of the calculated density of states with the XPS spectra of Erbudak *et al.* (*22*), in which the O-2*p* structure is more well resolved, shows even better agreement. This lends considerable credence to the overall correctness of the procedure used in determining the density-of-states of NbO. It also confirms the assumption that various simplifications introduced in the calculational schemes are physically reasonable. The results so far described should therefore form an adequate basis for prediction

TABLE II

COMPARISON OF NbO TRANSPORT PARAMETERS AT 100 kG MAGNETIC FIELD

Parameter	Temperature (K)[a]	Experimental range[b]	Calculated range[c]
$\Delta\rho/\rho_0$	78(100)	0.10–0.35	0.000015
	295(300)	0.01–0.09	<0.000001
R_I	78(100)	−6.8 –+3.0	+5.3–+6.0
	295(300)	−1.6 –+12	+5.4–+6.1

[a] Value in parentheses is the temperature at which calculated results apply.

[b] For samples 3–10 of Ref. (*3*); R_I values are to be multiplied by 10^{-15} for Gaussian units.

[c] R_I values are to be multiplied by 10^{-26}.

of transport coefficients, which is taken up below. Differences between the calculated density-of-states and experimental X-ray photoelectron spectra could be due to resolution limitations of the XPS instruments or to the tendency of XPS to reflect the properties of predominantly surface electrons.

There is, however, one somewhat unsatisfactory discrepancy between the current calculations and experimental findings. This pertains to the work function, which was estimated to be 6.5 eV. in the experimental work of Honig *et al.* (*21*), as compared to the calculated value of 9.4 eV. This disagreement may be due to assumed one-electron charge transfer between Nb and O, which was not decreased due to the difficulty of handling nonintegral charge transfers. Also, the same comments about XPS made above apply to its determination of the work function.

Finally, transport parameters predicted in magnetic field can be compared with measurements of Honig *et al.* (*3*). The calculated and observed ranges of transport parameters are shown in Table II, where $\Delta\rho/\rho_0$ represents the magnetoresistance and R_I the isothermal Hall coefficient. The calculated Hall coefficients are within the observed ranges, but the magnetoresistances observed are larger than calculated by a factor of about 10,000. Several possible effects observed in metals may be cited to explain this discrepancy.

Several metals (potassium, indium, aluminum, among others) have been observed to display nonsaturating magnetoresistance in large magnetic field which is much larger than the magnetoresistance predicted by traditional Boltzmann equation transport theory formulations (see Beers *et al.* (*23*), Lass (*24*)). The magnitude of the effect is very sensitive to sample preparation and handling and a detailed explanation has not yet been agreed upon. Lass (*24*) eliminated surface and connection effects as possible causes in potassium and found that the magnitude of the effect (as measured by the slope of the magnetic field dependence, called the Kohler slope) was influenced by time if the samples were kept at room temperature. Overhauser (*25*) has suggested that the effect in potassium is due to open orbits arising from the possible presence of charge-density waves. It is doubtful that this explanation applies to NbO.

Alternative explanations, both classical and quantum-mechanical, have been advanced to account for linear magnetoresistance effects in other metals. Herring (*26*) proposed an approach based on classical electrodynamic calculation of the effect of randomly placed inclusions and/or crystal defects, which are known to exist in all experimental samples. In NbO, the wide deviations from exact stoichiometry make presence of defects in off-stoichiometry material especially likely. Additionally, Herring observed that quantization into Landau levels or the effect of nonclosed Fermi surfaces could contribute to nonsaturation in the magnetoresistance. It is difficult to make a statement about the closed nature of the NbO Fermi surface based on the results quoted here.

It was calculated that a 0.1 to 1% volume fraction of nonconducting voids would be

required to explain the observed Kohler slopes by Herring's classical analysis (Stroud and Pan (*27*), Sampsell and Garland (*28*)). Beers (*23*) verified Herring's proposal experimentally in indium, but observed slight discrepancies in some geometries. This observation, combined with the large calculated void fractions, prompted the advancement of the quantum-mechanical theories mentioned below.

Van Gelder (*29*) proposed that magnetically bound states on inclusion surfaces could magnify the effect of the inclusion. Hsu and Falicov (*30*) found that a linear magnetoresistance could be generated by the magnetic field magnitudes used by Honig *et al.* (*3*). Arora (*31*) predicted that replacement of the Boltzmann equation with a quantum-mechanical formulation could yield linear magnetoresistance even in a perfect lattice.

Thus, a large number of candidate explanations exists for the anomalous magnetoresistance in NbO, mostly tied to imperfections in composition, measurement, crystal structure, or sample preparation. Since no special precautions were taken by Honig *et al.* (*3*) to eliminate strain from the samples, ensure composition control, or avoid surface and crystal imperfections (in fact, the samples were known to be nonstoichiometric) is it likely that one or more of the mechanisms above was active. This could explain the observed factor of 10,000 discrepancy between the measured and calculated magnetoresistances. It is hoped that future, more controlled work will clarify the causes of linear magnetoresistance and will provide additional data against which the predictions in this paper can be compared.

Acknowledgment

The author acknowledges the valuable assistance of Professor Jurgen M. Honig of Purdue University in formulating and executing this work.

References

1. J. M. Honig, G. V. Chandrashekhar, and J. Moyo, *J. Solid State Chem.* **2,** 528 (1970).
2. C. N. R. Rao, W. E. Wahnsiedler, and J. M. Honig, *J. Solid State Chem.* **2,** 315 (1970).
3. J. M. Honig, W. E. Wahnsiedler, and P. C. Eklund, *J. Solid State Chem.* **6,** 203 (1973).
4. J. A. Robertson and R. A. Rapp, *J. Phys. Chem. Solids* **30,** 1119 (1969).
5. W. A. Harrison, "Pseudo-potentials in the Theory of Metals," pp. 79ff, Benjamin, New York (1966).
6. E. Wimmer, K. Schwarz, R. Podloucky, P. Herzig, and A. Neckel, *J. Phys. Chem. Solids* **43,** 439 (1982).
7. T. Loucks, "Augmented Plane Wave Method," Benjamin, New York (1967).
8. H. Rose, Pogg. Ann. **104,** 310 (1858); **112,** 984 (1861).
9. W. Meissner, H. Franz, and H. Westerhoff, *Ann. Phys.* **17,** 593 (1933).
10. E. R. Pollard, PhD. thesis, Massachusetts Institute of Technology (1968).
11. E. R. Pollard and T. B. Reed, "Solid State Research Report," Massachusetts Institute of Technology Lincoln Laboratory, No. 3, 18–20 (1969).
12. W. E. Wahnsiedler, PhD. thesis, Purdue University.
13. D. Liberman, J. T. Waber, and D. T. Cromer, *Phys. Rev.* **137,** A27 (1965).
14. R. Latter, *Phys. Rev.* **99,** 510 (1955).
15. V. Ern and A. C. Switendick, *Phys. Rev.* **137,** A1927 (1965).
16. J. C. Slater, *Phys. Rev.* **81,** 385 (1951).
17. C. G. Benson and F. van Zeggeren, *J. Chem. Phys.* 26, 1083 (1957).
18. L. Bouckaert, R. Smoluchowski, and E. Wigner, *Phys. Rev.* **50,** 58 (1936).
19. J. C. Slater, "Quantum Theory of Molecules and Solids," Vol. 1, McGraw–Hill, New York (1963).
20. T. C. Harman and J. M. Honig, "Thermoelectric and Thermomagnetic Effects and Applications," McGraw–Hill, New York (1967).
21. J. M. Honig, A. P. B. Sinha, W. E. Wahnsiedler, and H. Kuwamoto, *Phys. Status Solidi* **73,** 651 (1976).
22. M. Erbudak, V. Gubanov, and E. Kurmaev, *J. Phys. Chem. Solids* **39,** 1157 (1978).
23. C. J. Beers, J. C. M. van Dongen, H. van Kempen, and P. Wyder, *Phys. Rev. Lett.* **40,** 1194 (1978).
24. C. S. Lass, *J. Phys. C (Solid State Phys.)* **3,** 1926 (1970).

25. A. W. OVERHAUSER, *Phys. Rev. B* **3,** 3173 (1971).
26. C. HERRING, *J. Appl. Phys.* **31,** 1939 (1960).
27. D. STROUD AND F. P. PAN, *Phys. Rev. B* **13,** 1434 (1976).
28. J. B. SAMPSELL AND J. C. GARLAND, *Phys. Rev. B* **13,** 583 (1976).
29. A. P. VAN GELDER, *Solid State Commun.* **28,** 481 (1978).
30. W. Y. HSU AND L. M. FALICOV, *Phys. Status Solidi B* **67,** 325 (1975).
31. V. K. ARORA, *Phys. Status Solidi B* **71,** 293 (1975).